Magnetic properties of ultrathin Si/Co/Ir(111) films

2008 J. Phys.: Condens. Matter 20 445003

(http://iopscience.iop.org/0953-8984/20/44/445003)

J. Phys.: Condens. Matter **20** (2008) 445003 (4pp) doi:10.1088/0953-8984/20/44/445003

Magnetic properties of ultrathin Si/Co/Ir(111) films

J S Tsay and Y C Liu

Department of Physics, National Taiwan Normal University, Taipei 116, Taiwan, Republic of China

E-mail: jstsay@phy.ntnu.edu.tw

Received 14 May 2008, in final form 29 August 2008
Published 25 September 2008
Online at stacks.iop.org/JPhysCM/20/445003

Abstract

A magnetic phase diagram for Si/Co/Ir(111) films has been established by the surface magneto-optic Kerr effect technique. The Si coverage, where ferromagnetism vanishes, increases from one monolayer to more than three monolayers as the coverage of the Co layer increases from two to five monolayers. As silicon is deposited on the surface of Co/Ir(111) films, Si atoms interact with the Co layer to form Si–Co compounds. The rough Si/Co interface impedes the motion of domain walls during the magnetization reversal process, thus increasing the coercive force. The formation of nonmagnetic Co–Si compounds reduces the effective magnetic layers, leading to a decrease in Kerr intensity and superparamagnetic behavior of the films.

1. Introduction

Metal–semiconductor interfaces have received much attention in the past decade because of the particular importance of developing the next-generation magnetic storage and semiconductor-based spintronics devices [1–5]. Considerable effort has been devoted to the study of metals on semiconductors [5–12]. There are relatively fewer reports discussing the inverse system, i.e. semiconductors on metals [4]. As compared with the metal-on-semiconductor interface, the semiconductor-on-metal interface is much narrower, and narrow interfaces show advantages in the fabrication of smaller devices in high-density integrated circuits [13, 14].

Silicon is of great importance in the semiconductor industry while cobalt is widely used in magnetic recording media. Extensive studies have been performed on cobalt deposited on Si substrates [5–10]. On an Si(111)-7 × 7 surface, direct evidence for the formation of $CoSi_2$ compounds at the interface was found and the interfacial effects caused the easy axis of magnetization of a Co/Si interface to be canted out of plane [5]. For Co deposited on Si(100) at room temperature, evidence of the out-diffusion of Si is seen for two monolayers (ML), which results in the formation of a CoSi phase [6]. A good-quality Si thin film was achieved by metal-induced Si growth on the Co silicide template [7]. A pseudo-layer-by-layer growth mode is proposed for describing the growth of Co on H-terminated Si surfaces because of the increase in surface mobility of Co adatoms in the presence of hydrogen [8]. Iridium is one of the most important materials as the preferred metal electrode because of its high resistance to corrosion and excellent stability at high temperatures [15]. For Co/Ir(111) films, a compositional anomaly of a great amount of adsorbed oxygen in submonolayer Co coverage occurs because of the maximized number of adsorption and incorporation sites for oxygen on the surface [16].

In this paper, we report on the magnetic properties of ultrathin Si/Co/Ir(111) films with Si ($x < 3$ ML) and Co ($y < 5$ ML) of different thicknesses. As silicon is deposited on the surface of Co/Ir(111) films, Si atoms interact with the Co layer to form Si–Co compounds. Both the coercive force and magneto-optic response of the Co/Ir(111) films are influenced by Si overlayers. A magnetic phase diagram of Si/Co/Ir(111) films has been successfully established.

2. Instrumentation

Experiments were carried out in an ultrahigh vacuum (UHV) chamber with a base pressure of 2×10^{-10} Torr. The UHV chamber is equipped for measurements of Auger electron spectroscopy (AES), low-energy electron diffraction (LEED), quadrupole mass spectroscopy (QMS) and the surface magneto-optic Kerr effect (SMOKE). An Ir(111) substrate was cleaned with cycles of Ar^+ ion bombardment and annealing treatments. The sputtering–annealing cycles were continued until a well-ordered 1 × 1 LEED pattern with bright, sharp

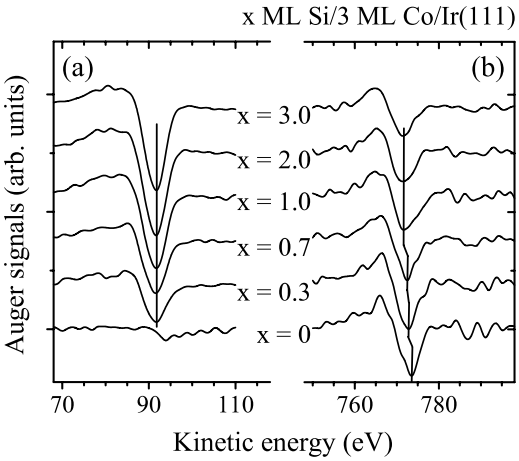

Figure 1. AES spectra near the (a) Si $L_3M_{23}M_{23}$ and (b) Co $L_3M_{45}M_{45}$ transitions for x ML Si/3 ML Co/Ir(111) films. As Si coverage increases, the kinetic energy of the Si $L_3M_{23}M_{23}$ transition line remains the same while the kinetic energy of the Co $L_3M_{45}M_{45}$ transition line decreases in the submonolayer range.

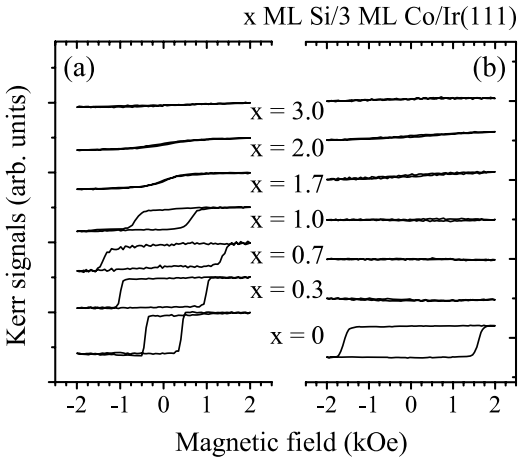

Figure 2. Kerr signals for x ML Si/3 ML Co/Ir(111) films in both (a) polar and (b) longitudinal configurations.

spots and a low background was observed. The chemical impurity of the surface was checked by AES. High purity cobalt (99.997%) was evaporated from a resistively heated cobalt coil. Silicon overlayers were prepared using an effusion cell of the DCA Instrument. All the films investigated were grown at ambient temperature. The coverages of the overlayers were determined by AES and double-checked by a thickness monitor. The surface of the Ir single crystal was cleaned after each experiment involving cobalt and silicon overlayers. The residual gas was monitored by the QMS. A He–Ne laser with a wavelength of 632.8 nm was used as the light source for the SMOKE measurements. The magnetic field was applied in-plane and perpendicular to the specimen surface for the longitudinal and polar Kerr effect configurations, respectively. The experiment set-up has been described in detail elsewhere [5, 16].

3. Results and discussion

As silicon is deposited on the surface of Co/Ir(111) films at ambient temperatures, chemical interaction between Si overlayers and Co films occurs. As an example for Si/3 ML Co/Ir(111), AES spectra near the (a) Si $L_3M_{23}M_{23}$ and (b) Co $L_3M_{45}M_{45}$ transitions are shown in figure 1 for Si coverage up to 3 ML. Before Si deposition, the Co $L_3M_{45}M_{45}$ Auger line occurs around 773.5 eV for 3 ML Co/Ir(111). As Si coverage increases in the submonolayer range, the Co Auger line shifts to lower kinetic energies. For an Si overlayer thicker than 1 ML, the shift is up to 2 eV. Shifts of the Auger line show that Co atoms are in different chemical environments [17]. Lower kinetic energy of the Co Auger line after the deposition of Si overlayers is attributed to the larger electron affinity of Si than that of Co, while intermixing of Si and Co occurs at the interface [18]. Before Si deposition, a bump appears around 94 eV as shown in figure 1(a), which corresponds to the Co $M_1M_4M_4$ transition line. After deposition of 0.3 ML Si, the Si $L_3M_{23}M_{23}$ transition line appears at 91.7 eV, which corresponds to the formation of Co–Si compounds. As Si coverage increases up to 3 ML, the kinetic energy of the Si $L_3M_{23}M_{23}$ transition line remains the same. This result indicates that the deposited Si atoms (<3 ML) are chemically active for the formation of Co–Si interfaces.

From SMOKE measurements, the coercive force for Co/Ir(111) films in the longitudinal configuration is several times that in the polar configuration. The present observation suggests the presence of two magnetically independent fractions of the film with out-of-plane and in-plane easy axes. As an example for 3 ML Co/Ir(111) shown in figure 2, the coercive force is about 0.4 kOe in the polar configuration while that in the longitudinal configuration is about four times this value. After deposition of 0.3 ML Si, magnetic hysteresis was detected only in the polar configuration. Figure 2 shows Kerr signals for x ML Si/3 ML Co/Ir(111) films in both polar and longitudinal configurations. As Si coverage increases, the shape of the hysteresis loops changes. The magnetic hysteresis is missing in the longitudinal configuration. This can be caused by an increasing coercive force exceeding the maximum available field and thus hiding the still-present in-plane magnetization. The silicide formation may turn an increasing part of the former out-of-plane fraction into a fraction with an in-plane easy axis.

The Kerr intensities and coercive force for x ML Si/3 ML Co/Ir(111) films in the polar configuration are summarized in figure 3. As Si coverage increases, the saturation Kerr intensity decreases monotonically until a zero value at 2.3 ML Si. This could be explained by the formation of nonmagnetic Co–Si compounds that reduce the effective magnetic layers. In addition, before the disappearance of the hysteresis for 1.7 and 2.0 ML Si/3 ML Co/Ir(111), the magnetization curves are slim as shown in figure 2. Both the remanent Kerr intensity and coercive force are close to a zero value. This represents the superparamagnetic behavior of films whose sizes of pure cobalt islands are greatly reduced. After deposition of submonolayer Si on the surface, the coercive force increases. This is attributed to the defects introduced at the Si/Co interface, which impede the motion of domain walls during the

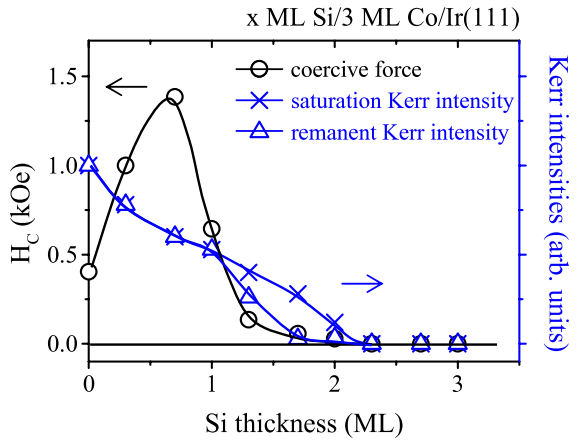

Figure 3. Kerr intensities and coercive force for x ML Si/3 ML Co/Ir(111) films in the polar configuration. As Si coverage increases, Kerr intensities decrease until a zero value at 2.3 ML Si.
(This figure is in colour only in the electronic version)

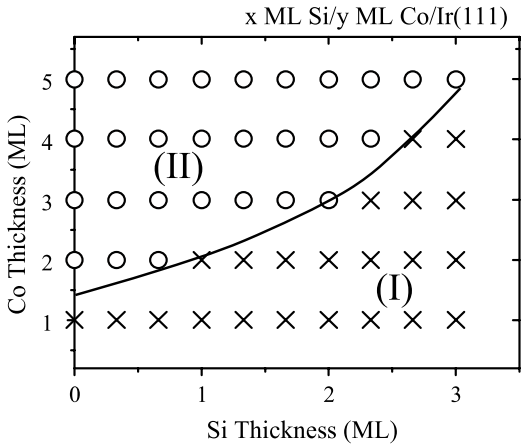

Figure 4. Magnetic phases for x ML Si/y ML Co/Ir(111) films. Nonmagnetic phase occurs in region I for thinner Co layers and thicker Si overlayers. In region II, the films are ferromagnetic.

magnetization reversal process. From our LEED experiments, a diffused 1 × 1 LEED pattern was observed after deposition of 0.3 ML Si. Thicker Si overlayers cause a strong background and no LEED spot can be observed, indicating that the Si–Co interface is disordered in long range.

A series of SMOKE measurements have been performed for Co (y < 5 ML) and Si (x < 3 ML) of different thicknesses. The decrease in polar Kerr intensity after deposition of Si overlayers for each Co coverage is similar to that of 3 ML Co/Ir(111) as shown in figure 3. The reason is that the formation of nonmagnetic Co–Si compounds reduces the effective Co layers. However, the Si coverage, where ferromagnetism vanishes, increases from 1 ML to more than 3 ML as the coverage of the Co layer increases from 2 to 5 ML. For all Co coverages (<5 ML) investigated, either no hysteresis occurs in the longitudinal configuration or a larger coercivity is observed in the longitudinal configuration than that in the polar configuration. A magnetic phase diagram for x ML Si/y ML Co/Ir(111) films was deduced from SMOKE measurements and is depicted in figure 4. In the regions labeled I for thinner Co and thicker Si layers, the films are nonmagnetic because Si adatoms interact with Co layers to form nonmagnetic compounds. In region II for thicker Co layers and thinner Si overlayers, the films are ferromagnetic.

4. Conclusion

We report the formation of interfacial compounds and the magnetic properties as silicon is deposited on the surface of Co/Ir(111) films. As Si coverage increases in the submonolayer range, the Co $L_3M_{45}M_{45}$ Auger line shifts to lower kinetic energies. This shows that Si interacts with the Co layer to form Si–Co compounds. According to the LEED experiments, the Si–Co interface is disordered in the long range. The defects introduced at the Si/Co interface impede the motion of domain walls during the magnetization reversal process and increase the coercive force. The formation of nonmagnetic Co–Si compounds reduces the effective magnetic layers and results in a monotonic decrease in saturation Kerr intensity until zero. A magnetic phase diagram for Si/Co/Ir(111) films with Co (y < 5 ML) and Si (x < 3 ML) of different thicknesses has been established. The Si coverage, where ferromagnetism vanishes, increases from 1 ML to more than 3 ML as Co coverage increases from 2 to 5 ML.

Acknowledgments

The authors would like to acknowledge the financial support from the National Science Council of ROC under grant nos. NSC 95-2112-M-003-023-MY2 and NSC-97-2112-M-003-010-MY3.

References

[1] Barth J V, Costantini G and Kern K 2005 *Nature* **437** 671
[2] Kubo O, Shingaya Y, Aono M and Nakayama T 2006 *Appl. Phys. Lett.* **88** 233117
[3] Schmitt A L, Zhu L, Schmeisser D, Himpsel F J and Jin S 2006 *J. Phys. Chem.* B **110** 18142
[4] Tsay J S, Yang A B, Wu C N and Shiu F S 2007 *Surf. Sci.* **601** 4265
[5] Tsay J S, Fu T Y, Lin M H, Yang C S and Yao Y D 2006 *Appl. Phys. Lett.* **88** 102506
[6] Dash S P, Goll D and Carstanjen H D 2007 *Appl. Phys. Lett.* **90** 132109
[7] Kim J, Piwowar A M, Nowak R, Gradella J A, Joseph A J and Anderson W A 2007 *Appl. Surf. Sci.* **253** 3053
[8] Pan J S, Liu R S, Zang Z, Poon S W, Ong W J and Tok E S 2006 *Surf. Sci.* **600** 1308
[9] Reader A H, Vanommen A H, Weijs P J W, Wolters R A M and Oostra D J 1993 *Rep. Prog. Phys.* **56** 1397
[10] Istratov A A and Weber E R 1998 *Appl. Phys.* A **66** 123
[11] Kaganer V M, Jenichen B, Shayduk R and Braun W 2008 *Phys. Rev.* B **77** 125325
[12] Su C W, Tsay J S and Yao Y D 2008 *Thin Solid Films* **516** 1164

[13] Lyubinetsky I V and Adamchuk V K 1996 *Thin Solid Films* **288** 182
[14] Chang Y, Hwu Y, Hansen J, Zanini F and Margaritondo G 1989 *Phys. Rev. Lett.* **63** 1845
[15] Liu Z P, Jenkins S J and King D A 2004 *J. Am. Chem. Soc.* **126** 10746
[16] Tsay J S and Chen Y S 2006 *Surf. Sci.* **600** 3555
[17] Ertl G and Küppers J 1985 *Low Energy Electrons and Surface Chemistry* 2nd edn (Weinheim: VCH) pp 37–40
[18] Lide D R 2003 *CRC Handbook of Chemistry and Physics* (New York: CRC Press)